Electrochemistry

# Realization of an Asymmetric Non-Aqueous Redox Flow Battery through Molecular Design to Minimize Active Species Crossover and Decomposition

Anuska Shrestha,[a] Koen H. Hendriks,[a] Mathew S. Sigman,[b] Shelley D. Minteer,[b] and Melanie S. Sanford*[a]

**Abstract:** This communication presents a mechanism-based approach to identify organic electrolytes for non-aqueous redox flow batteries (RFBs). Symmetrical flow cell cycling of a pyridinium anolyte and a cyclopropenium catholyte resulted in extensive capacity fade due to competing decomposition of the pyridinium species. Characterization of this decomposition pathway enabled the rational design of next-generation anolyte/catholyte pairs with dramatically enhanced cycling performance. Three factors were identified as critical for slowing capacity fade: (1) separating the anolyte–catholyte in an asymmetric flow cell using an anion exchange membrane (AEM); (2) moving from monomeric to oligomeric electrolytes to limit crossover through the AEM; and (3) removing the basic carbonyl moiety from the anolyte to slow the protonation-induced decomposition pathway. Ultimately, these modifications led to a novel anolyte–catholyte pair that can be cycled in an AEM-separated asymmetric RFB for 96 h with >95% capacity retention at an open circuit voltage of 1.57 V.

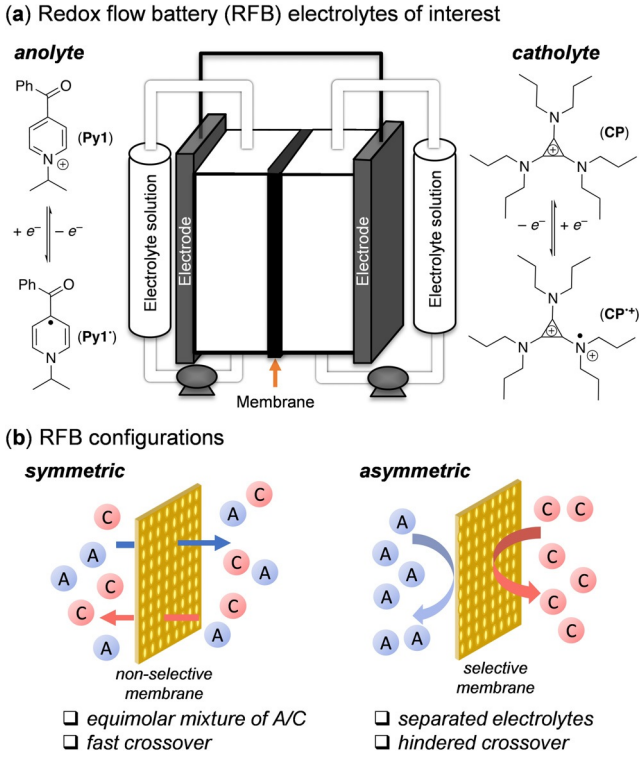


**Figure 1.** a) A schematic representation of a redox flow battery (RFB) and electrolytes of interest; b) Symmetric and asymmetric configurations for RFB operation (A = anolyte; C = catholyte).

The widespread adoption of renewable energy sources remains limited by a dearth of cost-effective and scalable methods for electrical energy storage.[1] Redox flow batteries (RFBs) represent an attractive technology to address this challenge.[2] In RFBs, energy is stored in solutions of redox active electrolytes (termed catholytes and anolytes) that undergo charge and discharge at inert electrodes (Figure 1a). This configuration facilitates scaling of these systems, since power and storage capacity are dictated by independent factors (the area/number of electrodes and the volume of the solutions, respectively). RFBs are also highly modular, as a wide variety of different anolytes–catholytes have been identified and their properties can be tuned by chemical modification.[3]

RFBs that consist of organic electrolytes in non-aqueous media have emerged as attractive targets, as they offer the possibility for wide potential windows and tailoring of the structures–properties of the organic active species.[4] To this end, recent work has uncovered a variety of organic anolyte and catholyte candidates with promising individual properties (e.g., redox potentials, cycling stabilities, solubilities).[5] Nonetheless, the integration of these organic anolyte–catholyte pairs into fully operational non-aqueous flow batteries remains a significant challenge. This is because RFBs containing two different active materials often suffer from chemical–electrochemical compatibility issues, resulting in parasitic decay of the electrolytes.[6] Although numerous examples of electrolyte incompatibilities have been documented, to date, few strat-

[a] A. Shrestha, Dr. K. H. Hendriks, Prof. M. S. Sanford
Joint Center for Energy Storage Research
Department of Chemistry, University of Michigan
930 North University Avenue, Ann Arbor, MI 48104 (USA)
E-mail: mssanfor@umich.edu
[b] Prof. M. S. Sigman, Prof. S. D. Minteer
Joint Center for Energy Storage Research, Department of Chemistry
University of Utah, 315 South 1400 East, Salt Lake City, UT 84112 (USA)
Supporting information and the ORCID identification number(s) for the author(s) of this article can be found under:
https://doi.org/10.1002/chem.202000749.

egies have been developed to characterize and mitigate these processes.[5]

This communication describes a detailed investigation of the flow cell cycling of an organic anolyte–catholyte pair developed by our team. Although the pyridinium anolyte **Py1**[5a] and cyclopropenium catholyte **CP**[5b,c] (Figure 1a) are each stable when cycled independently, we demonstrate that they exhibit extensive decomposition when cycled together in an electrochemical flow cell. A detailed analysis of the decay pathway is presented, and these insights are used to design new electrolytes that mitigate this process. Ultimately, iterative modifications led to next-generation electrolytes that exhibit more than an order-of-magnitude enhancement in capacity retention during flow cell cycling.

**Py1**[7] and **CP** each undergo stable individual cycling in MeCN/$KPF_6$ (>200 charge-discharge cycles over 36–48 h).[5] As such, a next step is to pair these materials in a flow cell. The standard configuration for a non-aqueous flow battery involves an equimolar mixture of anolyte and catholyte on both sides of the cell in conjunction with a microporous polymer separator (Figure 1b, symmetric).[8] This symmetric configuration requires compatibility between the anolyte and catholyte, which can be preliminarily assessed by cyclic voltammetry (CV).[7] The CV of a 1:1 mixture of **Py1** and **CP** (5 mM in MeCN/$KPF_6$) reveals no difference from the individual CV of each molecule (Figure 2a). Furthermore, minimal change is observed after 10 CV cycles, indicating that **Py1** and **CP** are compatible on the CV timescale.

On the basis of these CV data, we moved forward with flow cell cycling of a 1:1 mixture of **Py1** and **CP**. Our flow cell[9] consists of graphite charge collecting plates with an interdigitated flow field, in combination with 400 μm thick carbon felt electrodes and a microporous Celgard 2500 separator. The electrolyte solutions (6 mL total volume in each chamber of a 50 mM concentration of each active species in 0.5 M $KPF_6$ in MeCN) are flowed at 10 mL $min^{-1}$ and are subjected to galvanostatic cycling at 10 mA $cm^{-2}$ over the first redox couple of **Py1** (at −1.02 V vs. $Ag/Ag^+$). This results in a cell voltage of 1.90 V. As shown in Figure 2b, despite the promising CV data, this system shows modest cycling performance. It initially charges to just 62% of the theoretical capacity and then fades by 62% over 55 h of cycling (Figure 2b). CV analysis of the spent solutions show that this fade is largely due to decomposition of the anolyte (Figure S5).

We first focused on characterizing the anolyte decomposition pathway. One and two dimensional $^1H$ NMR spectroscopic

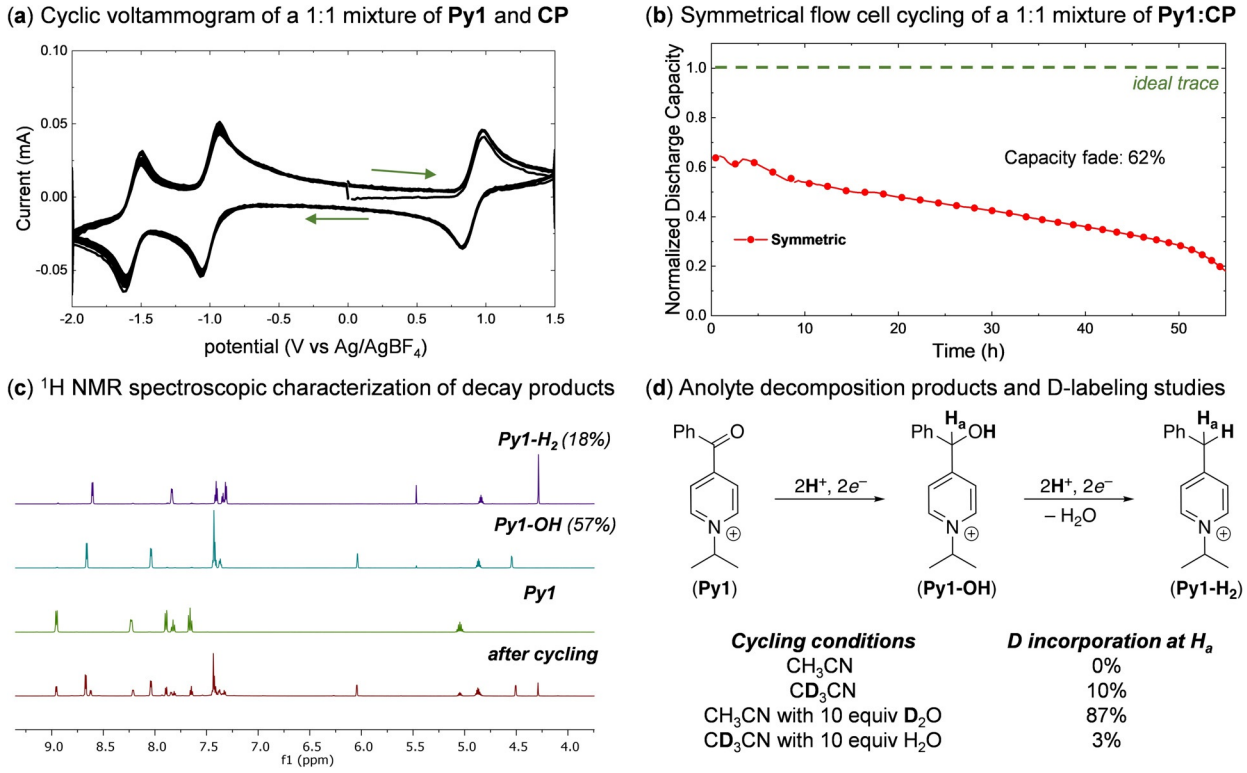


**Figure 2.** (a) Cyclic voltammogram of an equimolar solution of **Py1** and **CP** for 10 continuous cycles. Cyclic voltammetry was conducted using glassy carbon as working electrode, Pt-wire as counter electrode and $Ag/AgBF_4$ as reference. (b) Symmetrical electrochemical cycling of **Py1**/**CP** in a prototype RFB. Figure 1a shows the transformations occurring during the cycling process. Experiment conducted with each reservoir containing 6 mL of a 50 mM solution of the respective redox active species in 0.5 M $KPF_6$ in acetonitrile. The solutions were flowed at 10 mL $min^{-1}$, and the battery was charged–discharged with a current density of 10 mA $cm^{-2}$. Normalized discharge capacity (normalized against maximum theoretical capacity) is plotted against time. (c) Identification of anolyte decomposition through $^1H$ NMR spectra analysis of the spent solution (after cycling) and comparative analysis of the spent solution with the independently synthesized **Py1-OH** and **Py1-$H_2$**. (d) Pathway for anolyte decomposition during the electrochemical cycling and deuterium labeling experiments to identify the source of anolyte decomposition. Deuterium labeling experiments were performed in a symmetric system with **CP** as catholyte. **Py1-$H_2$** was not detected under these conditions.

analysis of the spent electrolyte solutions showed that 74% of the anolyte is transformed into an approximately 3:1 mixture of two new compounds: a major species (**Py1-OH**, 57%) and minor species (**Py1-H$_2$**, 18% Figure 2c).[10,11] As shown in Figure 2d, **Py1-OH** derives from a two proton–two electron reduction of **Py-1**, whereas **Py1-H$_2$** derives from a two proton–two electron reduction of **Py1-OH** accompanied by loss of water.[12,13]

Deuterium labeling studies were conducted to determine the origin of the protons in this system (Figure 2d). When $CD_3CN$ was used as the solvent for cycling, 10% deuteration was detected at $H_a$ of **Py1-OH**. In contrast, in $CH_3CN$ with 10 equivalents of added $D_2O$ under otherwise analogous conditions, 87% deuteration was observed. These results suggest that the protons predominantly derive from adventitious water, which we were unable to completely remove even upon rigorous drying of the electrolyte solutions. Importantly, the decomposition of **Py1** to **Py1-OH** and **Py1-H$_2$** is greatly accelerated by the presence of oxidized **CP**. When **Py1** is subjected to flow cell cycling in $CH_3CN$ under analogous conditions but in the absence of **CP**, only traces of **Py1-OH** or **Py1-H$_2$** are detected.[10] These results suggest that decomposition of the anolyte can be attenuated through the implementation of an asymmetric cell (Figure 1b), in which **Py1** and **CP** are physically separated during electrochemical cycling. This asymmetric configuration requires a membrane that can impede the crossover of redox active species while maintaining fast equilibration of charge-balancing ions. We reasoned that the cationic electrolytes **Py1** and **CP** could be effectively separated using an organic compatible anion exchange membrane (AEM)[14] such as Fumasep FAPQ-375-PP.[15] As such, an asymmetric flow battery was assembled with 50 mM solutions of **Py1** and **CP** separated by Fumasep FAPQ-375-PP. Encouragingly, this system demonstrated improved cycling performance relative to the original symmetric cell (compare black data in Figure 3c to data in Figure 2b). It initially charged to >80% of the theoretical capacity and then faded by 50% over 96 h of cycling. NMR spectroscopic analysis of the spent electrolyte solutions revealed a significant enhancement in anolyte stability in this asymmetric system. Only 26% decomposition of **Py1** was observed over the 96 h of cycling, which compares favorably to 74% decomposition over just 55 h of cycling in the symmetric RFB. In-

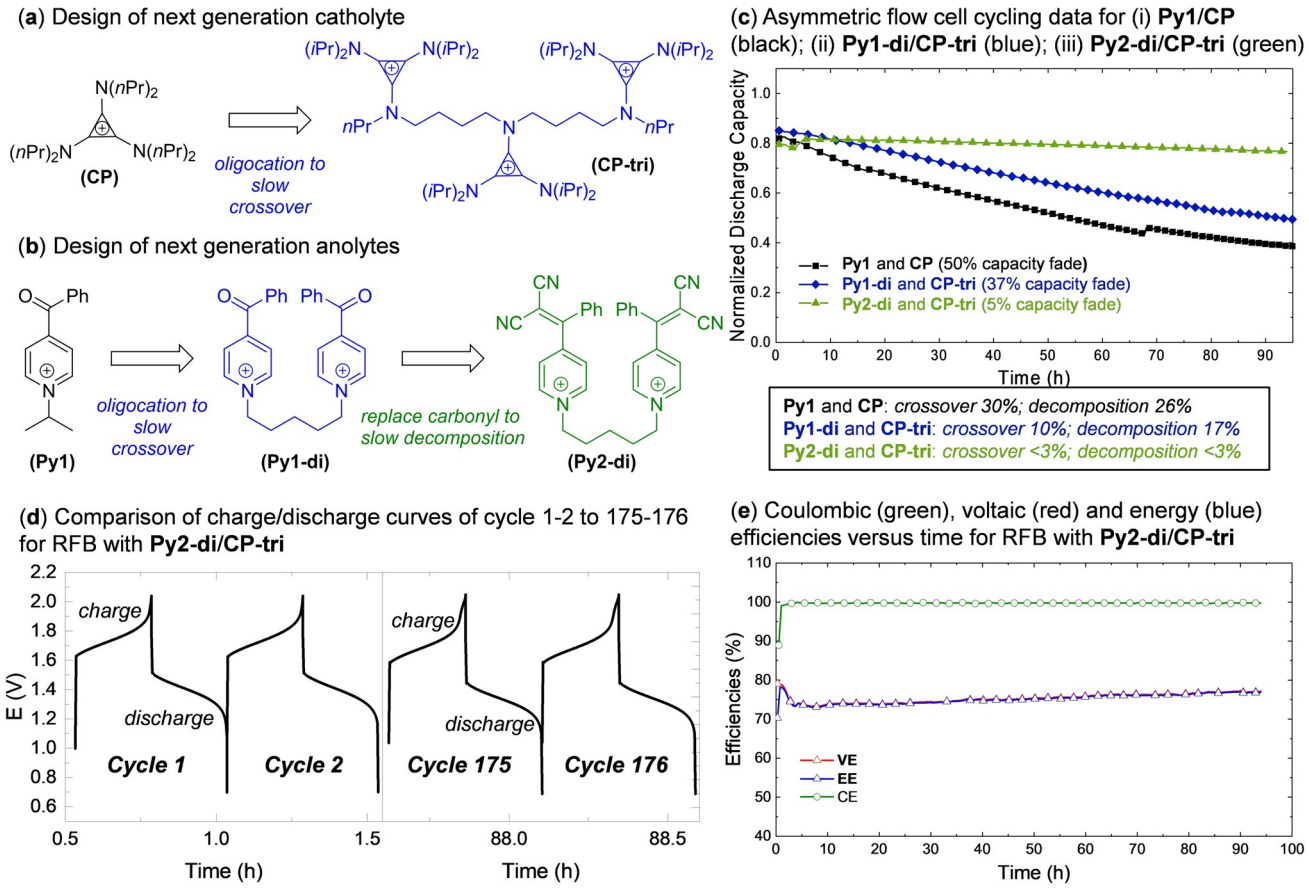


**Figure 3.** Molecular design to identify a new generation of (a) catholyte (**CP**) to trimer (**CP-tri**) to prevent crossover and (b) anolyte (**Py1**) to dimer (**Py1-di**) to prevent crossover and subsequently to protected dimer (**Py2-di**) to prevent decomposition of the anolyte. (c) Electrochemical performance of **Py1**/**CP**, **Py1-di**/**CP-tri** and **Py2-di**/**CP-tri** in asymmetric batteries. Figure 1a shows the transformations occurring during the cycling process. Experiment conducted with each reservoir containing 6 mL of a 50 mM solution of the respective redox active species in 0.5 M $KPF_6$ in acetonitrile. The solution was flowed at 10 mL min$^{-1}$, and the battery was charged/discharged with a current density of 10 mA cm$^{-2}$. Normalized discharge capacity (normalized against maximum theoretical capacity) is plotted against time. (d) Comparison of charge–discharge curves of early cycles (1–2) to later cycles (175–176) of the electrochemical cycling with **Py2-di**/**CP-tri**. (e) Coulombic (green), voltaic (red) and energy (blue) efficiencies of **Py2-di**/**CP-tri** battery versus time.

stead, the major cause of capacity fade is crossover of the active species through the AEM. CV analysis of the spent solutions shows 30% crossover of **CP** and 26% crossover of **Py1** over 96 h of cycling.

We hypothesized that crossover could be impeded by moving from the monocationic monomeric electrolytes to polycationic oligomers, which should exhibit enhanced electrostatic repulsions with the AEM. Notably, previous work has shown that oligomeric CP derivatives (e.g., **CP-tri** in Figure 3a) can be effectively separated using a size-exclusion membrane;[5c,16] however, to date, the feasibility of separating these polycations using AEMs has not been demonstrated. We initially targeted **CP-tri** in conjunction with the similarly designed pyridinium dimer **Py1-di** as second generation electrolytes for this system (Figure 3b).[17] Asymmetric cycling of **Py1-di**/**CP-tri** in a Fumasep FAPQ-375-PP-separated flow cell (Figure 3c, blue data) yielded an RFB with an open circuit potential of 1.95 V. As anticipated, electrolyte crossover was significantly reduced in this system. CV analysis of the spent solutions showed $<3\%$ crossover of **CP-tri** and approximately 10% crossover of **Py1-di** over the 96 h cycling experiment. This experiment demonstrates for the first time that AEMs can effectively separate cationic oligomers in non-aqueous RFBs. The decomposition of the anolyte was significantly attenuated relative to the monomeric system (17 versus 26%, respectively), likely due to the more effective separation. However, due to the low crossover, anolyte decomposition is again the leading cause of capacity fade in this second-generation asymmetric system.

A third-generation anolyte was designed to further limit decomposition of the anolyte during cycling. As discussed above, the conversion of **Py1** to **Py1-OH** involves a net two proton–two electron reduction, with the basic carbonyl moiety likely serving as the initial proton acceptor.[18] We reasoned that this undesired pathway could be attenuated by replacing the reactive carbonyl site with a less basic pseudo-oxocarbon malononitrile group ($C(CN)_2$).[19] The malononitrile analogue of **Py1-di** (**Py2-di**) was synthesized from benzoyl pyridine through a $TiO_2$-mediated condensation reaction followed by alkylation with dibromopropane.[20] The cyclic voltammogram of **Py2-di** shows two single electron redox couples at $-0.626$ and $-0.976$ V vs. $Ag/Ag^+$ (see Supporting Information).[21] This represents a 0.4 V increase in the redox potential compared to the ketone analogue **Py1-di** ($-1.01$ and $-1.55$ V vs. $Ag/Ag^+$). However, this is accompanied by a large enhancement in cycling stability. **Py2-di** has a solubility of 1.70 M per redox active unit in MeCN. Data for the asymmetric cycling of **Py2-di**/**CP-tri** in a Fumasep FAPQ-375-PP-separated flow cell is shown in Figure 3c (green data). This system yields an RFB with an open circuit voltage of 1.57 V. As a result of these modifications, only $\approx5\%$ fade of capacity is detected over 96 h of cycling ($\approx200$ charge–discharge cycles). $^1$H NMR spectroscopic analysis of the spent anolyte solution shows only traces ($\approx3\%$) of products analogous to **Py1-OH**. Additionally, minimal crossover of the polycations **CP-tri** ($<1\%$) or **Py2-di** ($<3\%$) is detected.

Overall, this study presents a mechanism-based approach to the molecular design of electrolytes for implementation in an asymmetric non-aqueous redox flow battery. Decomposition of the anolyte during battery cycling is demonstrated as a major factor contributing to capacity fade in both symmetric and asymmetric systems. The asymmetric configuration helps to mitigate this decomposition but introduces crossover as another contributor to capacity fade. Two key modifications were required to achieve stable cycling of an asymmetric RFB in this system. First, oligomerization of the electrolytes resulted in oligocations that resist crossover due to electrostatic repulsions with the anion exchange membrane. Second, proton-coupled anolyte decomposition was mitigated by the replacement of a basic carbonyl with a malonitrile group in the anolyte scaffold. Overall, these studies demonstrate that detailed chemical analysis of RFB systems coupled with iterative design and synthesis of next generation electrolytes is an effective strategy for advancing electrolyte candidates for this application.

## *Acknowledgements*

This work was supported by the Joint Center for Energy Storage Research (JCESR) a Department of Energy, Energy Innovation Hub. We thank Jonathan Ruchti and Marino Borjesson for helpful discussions.

## Conflict of interest

The authors declare no conflict of interest.

**Keywords:** anolyte decomposition · asymmetric · crossover · non-aqueous · redox flow batteries

[1] a) D. Larcher, J. Tarascon, *Nat. Chem.* **2015**, *7*, 19–29; b) T. M. Gür, *Energy Eviron. Sci.* **2018**, *11*, 2696–2767.
[2] a) G. L. Soloveichik, *Chem. Rev.* **2015**, *115*, 11533–11558; b) X. Wei, W. Pan, W. Duan, A. Hollas, Z. Yang, B. Li, X. Nie, J. Liu, D. Reed, W. Wang, V. Sprenkle, *ACS Energy Lett.* **2017**, *2*, 2187–2204; c) J. Noack, N. Roznyatovskaya, T. Herr, P. Fischer, *Angew. Chem. Int. Ed.* **2015**, *54*, 9776–9809; *Angew. Chem.* **2015**, *127*, 9912–9947; d) J. Rugolo, M. J. Aziz, *Energy Environ. Sci.* **2012**, *5*, 7151–7160; e) J. Winsberg, T. Hagemann, T. Janoschka, M. D. Hager, U. S. Schubert, *Angew. Chem. Int. Ed.* **2017**, *56*, 686–711; *Angew. Chem.* **2017**, *129*, 702–729; f) P. V. Kamat, K. S. Schanze, J. M. Buriak, *ACS Energy Lett.* **2017**, *2*, 1368–1369.
[3] a) Y. Ding, Y. Zhao, Y. Li, J. B. Goodenough, G. Yu, *Energy Environ. Sci.* **2017**, *10*, 491–497; b) B. Huskinson, M. P. Marshak, C. Suh, S. Er, M. R. Gerhardt, C. J. Galvin, X. Chen, A. Aspuru-Guzik, R. G. Gordon, M. J. Aziz, *Nature* **2014**, *505*, 195–198; c) K. Lin, R. Gomez-Bombarelli, E. S. Beh, L. Tong, Q. Chen, A. Valle, A. Aspuru-Guzik, M. J. Aziz, R. G. Gordon, *Nat. Energy* **2016**, *1*, 16102; d) T. Janoschka, N. Martin, M. D. Hager, U. S. Schubert, *Angew. Chem. Int. Ed.* **2016**, *55*, 14427–14430; *Angew. Chem.* **2016**, *128*, 14639–14643; e) B. Hu, C. DeBruler, Z. Rhodes, T. L. Liu, *J. Am. Chem. Soc.* **2017**, *139*, 1207–1214; f) T. B. Schon, B. T. McAllister, P. F. Li, D. S. Seferos, *Chem. Soc. Rev.* **2016**, *45*, 6345–6404.
[4] a) J. Zhang, Z. Yang, I. A. Shkrob, R. S. Assary, S. Tung, B. Silcox, W. Duan, J. Zhang, C. C. Su, B. Hu, B. Pan, C. Liao, Z. Zhang, W. Wang, L. A. Curtiss, L. T. Thompson, X. Wei, L. Zhang, *Adv. Energy Mater.* **2017**, *7*, 1701272; b) L. Su, M. Ferrandon, J. A. Kowalski, J. T. Vaughey, F. R. Brushett, *J. Electrochem. Soc.* **2014**, *161*, A1905–A1914; c) W. Wang, V. Sprenkle, *Nat. Chem.* **2016**, *8*, 204–206; d) W. Wang, Q. T. Luo, B. Li, X. L. Wei, L. Y. Li, Z. G. Yang, *Adv. Funct. Mater.* **2013**, *23*, 970–986; e) J. Winsberg, T. Hagemann, S. Muench, C. Friebe, B. Haupler, T. Janoschka, S. Morgenstem, M. D. Hager, U. S. Schubert, *Chem. Mater.* **2016**, *28*, 3401–3405; f) M. Burgess, J. S. Moore, J. Rodriguez-Lopez, *Acc. Chem. Res.* **2016**, *49*,

2649 – 2657; g) E. C. Montoto, G. Nagarjuna, J. S. Moore, J. Rodriguez-Lopez, *J. Electrochem. Soc.* **2017**, *164*, A1688 – A1694.
[5] a) C. S. Sevov, D. P. Hickey, M. E. Cook, S. G. Robinson, S. Barnett, S. D. Minteer, M. S. Sigman, M. S. Sanford, *J. Am. Chem. Soc.* **2017**, *139*, 2924 – 2927; b) C. S. Sevov, S. K. Samaroo, M. S. Sanford, *Adv. Energy Mater.* **2017**, *7*, 1602027; c) K. H. Hendriks, S. G. Robinson, M. N. Braten, C. S. Sevov, B. A. Helms, M. S. Sigman, S. D. Minteer, M. S. Sanford, *ACS Cent. Sci.* **2018**, *4*, 189 – 196; d) X. Wei, W. Xu, M. Vijayakumar, L. Cosimbescu, T. Liu, V. Sprenkle, W. Wang, *Adv. Mater.* **2014**, *26*, 7649 – 7653; e) B. Hu, T. L. Liu, *J. Energy Chem.* **2018**, *27*, 1326 – 1332.
[6] a) Q. Chen, L. Eisenach, M. J. Aziz, *J. Electrochem. Soc.* **2016**, *163*, A5057 – A5063; b) M. R. Gerhardt, E. S. Beh, L. Tong, R. G. Gordon, M. J. Aziz, *MRS Adv.* **2017**, *2*, 431 – 438; c) M.-A. Goulet, L. Tong, D. A. Pollack, D. P. Tabor, S. A. Odom, A. Aspuru-Guzik, E. E. Kwan, R. G. Gordon, M. J. Aziz, *J. Am. Chem. Soc.* **2019**, *141*, 8014 – 8019; d) L. Tong, Y. Jing, R. G. Gordon, M. J. Aziz, *ACS Appl. Energy Mater.* **2019**, *2*, 4016 – 4021; e) L. Tong, M.-A. Goulet, D. P. Tabor, E. F. Kerr, D. De Porcellinis, E. M. Fell, A. Aspuru-Guzik, R. G. Gordon, M. J. Aziz, *ACS Energy Lett.* **2019**, *4*, 1880 – 1887; f) J. Zhang, I. A. Shkrob, R. S. Assary, S. O. Tung, B. Silcox, L. A. Curtiss, L. Thompson, L. Zhang, *J. Phys. Chem. C* **2017**, *121*, 23347 – 23358.
[7] **Py1** was selected as the anolyte for these studies based on its synthetic accessibility (i.e., the synthesis of **Py1** is readily scalable and proceeds in 1 step from commercial materials).
[8] a) W. Duan, J. Huang, J. A. Kowalski, I. A. Shkrob, M. Vijayakumar, E. Walter, B. Pan, Z. Yang, J. D. Milshtein, B. Li, C. Liao, Z. Zhang, W. Wang, J. Liu, J. S. Moore, F. R. Brushett, L. Zhang, X. Wei, *ACS Energy Lett.* **2017**, *2*, 1156 – 1161; b) J. Huang, W. Duan, J. Zhang, I. A. Skrob, R. S. Assary, B. Pan, C. Liao, Z. Zhang, X. Wei, L. Zhang, *J. Mater. Chem. A* **2018**, *6*, 6251 – 6254; c) J. Huang, Z. Yang, M. Vijayakumar, W. Duan, A. Hollas, B. Pan, W. Wang, X. Wei, L. Zhang, *Adv. Sustainable Syst.* **2018**, *2*, 1700131; d) X. Wei, W. Duan, J. Huang, L. Zhang, B. Li, D. Reed, W. Xu, V. Sprenkle, W. Wang, *ACS Energy Lett.* **2016**, *1*, 705 – 711.
[9] a) J. D. Milshtein, A. P. Kaur, M. D. Casselman, J. A. Kowalski, S. Modekrutti, P. L. Zhang, N. H. Attanayake, C. F. Elliott, S. R. Parkin, C. Risko, F. R. Brushett, S. A. Odom, *Energy Environ. Sci.* **2016**, *9*, 3531 – 3543; b) J. D. Milshtein, J. L. Barton, R. M. Darling, F. R. Brushett, *J. Power Sources* **2016**, *327*, 151 – 159.
[10] Both of the decomposed compounds are reoxidized to the ketone in the presence of air.
[11] Control experiments reveal that neither **Py1** nor **Py-1**$^{\cdot}$ decompose to **Py1-OH** or **Py1-H$_2$** when stored for 96 h in 0.5 M $KPF_6$ in MeCN. Furthermore, $<5\%$ decomposition is observed over this timescale during half-cell electrochemical cycling of **Py1**. Leventis et al. have reported on similar decomposition products during the electrochemical cycling of pyridinium salts in the presence of proton donors. Similarly, we observe that half-cell electrochemical cycling of **Py1** in the presence of 5 equivalents of acetic acid leads to quantitative conversion to **Py1-OH**. Overall, this leads us to hypothesize that the radical cation of **CP** (generated during flow cell cycling in this system) reacts with adventitious water to generate protons, which then lead to the decay of the anolyte.
[12] Protonation has frequently been invoked as a parasitic reaction leading to decomposition of ROMs, particularly those containing a carbonyl moiety. See: a) S. K. Park, J. Shim, J. Yang, K. H. Shin, C. S. Jin, B. S. Lee, Y. S. Lee, J. D. Jeon, *Electrochem. Commun.* **2015**, *59*, 68 – 71; b) X. Wei, W. Xu, J. Huang, L. Zhang, E. Walter, C. Lawrence, M. Vijayakumar, W. A. Henderson, T. Liu, L. Cosimbescu, *Angew. Chem. Int. Ed.* **2015**, *54*, 8684 – 8687; *Angew. Chem.* **2015**, *127*, 8808 – 8811; c) R. Naef, *Helv. Chim. Acta* **1982**, *65*, 1734 – 1742.
[13] Similar decomposition is observed for *N*-ethyl-2,6-dimethyl-4-benzoylpyridinium, which was previously optimized for stability against radical dimerization (ref. [5a]).
[14] S.-H. Shin, S.-H. Yun, S.-H. Moon, *RSC Adv.* **2013**, *3*, 9095 – 9116.
[15] For recent examples of flow cell cycling with Fumasep FAPQ-375-PP in MeCN, see: a) Y. Yan, S. G. Robinson, M. S. Sigman, M. S. Sanford, *J. Am. Chem. Soc.* **2019**, *141*, 15301 – 15306; b) S. G. Robinson, Y. Yan, K. H. Hendriks, M. S. Sanford, M. S. Sigman, *J. Am. Chem. Soc.* **2019**, *141*, 10171 – 10176.
[16] a) M. J. Baran, M. N. Braten, E. C. Montoto, Z. T. Gossage, L. Ma, E. Chenard, J. S. Moore, J. Rodriguez-Lopez, B. A. Helms, *Chem. Mater.* **2018**, *30*, 3861 – 3866; b) S. E. Doris, A. L. Ward, A. Baskin, P. D. Frischmann, N. Gavvalapalli, E. Chenard, C. S. Sevov, D. Prendergast, J. S. Moore, B. A. Helms, *Angew. Chem. Int. Ed.* **2017**, *56*, 1595 – 1599; *Angew. Chem.* **2017**, *129*, 1617 – 1621.
[17] See Supporting Information for complete chemical and electrochemical characterization of **CP-tri** and **Py1-di**.
[18] N. Leventis, I. A. Elder, X. Gao, E. W. Bohannan, C. Sotiriou-Leventis, A. M. M. Rawashdeh, T. J. Overschmidt, K. R. Gaston, *J. Phys. Chem. B* **2001**, *105*, 3663 – 3674.
[19] a) K. D. Thériault, C. Radford, M. Parvez, B. Heyne, T. C. Sutherland, *Phys. Chem. Chem. Phys.* **2015**, *17*, 20903 – 20911; b) Z. Rappoport, *Isr. J. Chem.* **1970**, *8*, 749 – 751; c) K. Wallenfels, K. Friedrich, J. Rieser, W. Ertel, H. K. Thieme, *Angew. Chem.* **1976**, *88*, 311 – 320; d) L. M. Doane, A. J. Fatiadi, *Angew. Chem. Int. Ed. Engl.* **1982**, *21*, 635 – 636; *Angew. Chem.* **1982**, *94*, 649 – 650; e) Z.-M. Xue, C.-H. Chen, *Int. J. Quantum Chem.* **2007**, *107*, 637 – 646; f) C. G. Armstrong, R. W. Hogue, K. E. Toghill, *J. Power Sources* **2019**, *440*, 227037.
[20] M. Hosseini-Sarvari, H. Shargi, S. Etemad, *Chin. J. Chem.* **2007**, *25*, 1563 – 1567.
[21] The first and second reductions of **Py1-di** (to afford the neutral diradical species) occur at the same potential (−1.01 V). See Figure S1(b) for CV.

Manuscript received: February 11, 2020
Accepted manuscript online: February 12, 2020
Version of record online: April 15, 2020